Modelling Flow in a Fluidized Bed

Aryan Gupta

Sardar Vallabhbhai National Institute of Technology, Surat

Under the Guidance
Of

Dr. Raghvendra Gupta
Professor at Indian Institute of Technology, Guwahati

Nikhil Chitnavis
Ph.D. at the Indian Institute of Technology, Madras

Abstract

Fluidized bed technology is widely used in power generation and chemical processing due to its superior heat and mass transfer capabilities. This study focuses on simulating gas–solid flow in a fluidized bed using the Eulerian–Eulerian approach with OpenFOAM's 'twoPhaseEulerFoam' solver. The effects of drag models (Gidaspow and Syamlal) and boundary conditions on bed expansion and solid volume fraction were investigated. Simulation results were validated against experimental data from previous studies. Mesh and time-step sensitivity analyses indicated that a grid size of 0.005 m and a time step of 10^{-3} s offer an optimal balance between accuracy and computational cost. These findings highlight critical factors for improving the reliability and efficiency of fluidized bed simulations.

1. Introduction

Fluidized bed technology is widely used across various industries due to its superior heat and mass transfer capabilities. In a fluidized bed, solid particles are suspended in an upward-flowing gas or liquid, creating a fluid-like state that enhances mixing, temperature uniformity, and chemical reactions. This makes it highly effective for applications such as combustion, gasification, and drying processes. Its ability to handle diverse materials while maintaining energy efficiency and environmental compliance underscores its importance in modern engineering and manufacturing.

Despite its widespread application, modelling a fluidized bed remains a challenging task. The primary difficulty lies in the complex interplay of multiphase flow dynamics, particle-particle

interactions, and heat and mass transfer phenomena. The system involves gas-solid interactions where particles exhibit behaviours ranging from dense, bubbling regimes to fast fluidization or pneumatic transport, making it difficult to develop a universal model. Furthermore, factors such as particle size distribution, shape, and cohesion add to the complexity of predictions. Computational challenges also arise because accurately simulating millions of particles with realistic contact mechanics requires enormous computational resources, often necessitating simplifications that can compromise accuracy.

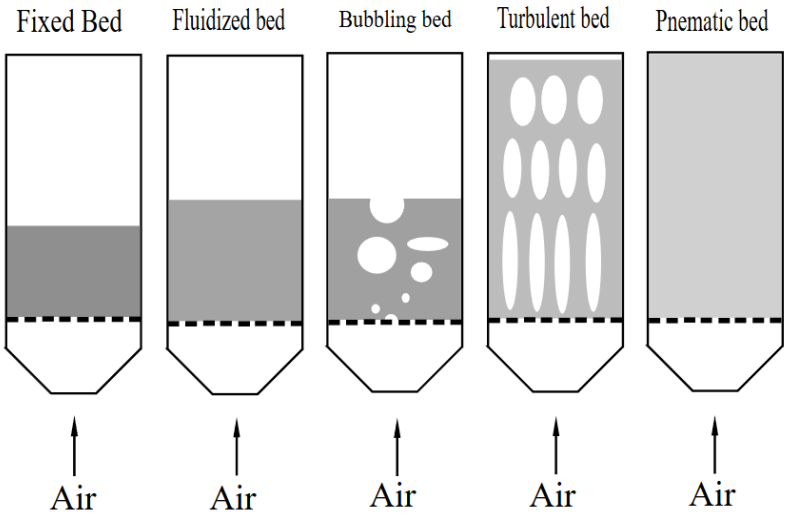

Figure 1: Types of Fluidization.

As seen in Figure 1, fluidization occurs at a certain inlet velocity of air. After increasing its velocity, the bed height rises a lot, and the shape of the bubble changes.

2. Problem Statement

In this work, the objective is to simulate the flow of solid particles in a fluidized bed using the *twoPhaseEulerFoam* solver in OpenFOAM, employing the Eulerian-Eulerian approach to model the gas and solid phases as interpenetrating continua. The study focuses on the following key challenges:

Comparing the simulated solid volume fraction fields with experimental and simulation data from Fariborz Taghipour (2005) and simulation data of Yefei Liu (2014) to validate the accuracy of the simulation. Investigate the effects of different drag models, Gidaspow (1994), and Syamlal (1993), on bed expansion and solid concentration predictions.

Examine the influence of different pairs of boundary conditions (fixedValue and zeroGradient) on the stability and realism of the simulation, particularly for the gas and solid phases at the inlet of the solid volume fraction. The outcomes of this study aim to provide insights into the optimal modelling strategies for fluidized beds, ensuring reliable predictions of flow behaviour while minimizing computational resources. The results will contribute to improving the design and operation of fluidized bed systems in industrial applications.

3. Governing equations

The simulation of a fluidized bed is done by solving the governing equations of momentum, mass, and energy conservation. For simulation, the open-source software OpenFOAM version 2312 is used, and within OpenFOAM, the twoPhaseEulerFoam solver is employed. The kinetic theory of granular flow is used as a closure of solid stress terms.

The continuity equation can be given as

$$\frac{\partial(\alpha_g \rho_g)}{\partial t} + \nabla \cdot (\alpha_g \rho_g \boldsymbol{U_g}) = 0 \quad (1)$$

$$\frac{\partial(\alpha_s \rho_s)}{\partial t} + \nabla \cdot (\alpha_s \rho_s \boldsymbol{U_s}) = 0 \quad (2)$$

α_g and α_s are the volumetric fractions of gas and solid phases; the sum of volume fractions of gas and solid is 1.

The momentum equations of the gas and solid phases are given as,

$$\frac{\partial(\alpha_g \rho_g U_g)}{\partial t} + \nabla \cdot (\alpha_g \rho_g U_g U_g) = -\alpha_g \nabla p + \nabla \cdot (\alpha_g \tau_g) + \alpha_g \rho_g g + \beta(U_s - U_g) \quad (3)$$

$$\frac{\partial(\alpha_s \rho_s U_s)}{\partial t} + \nabla \cdot (\alpha_s \rho_s U_s U_s) = -\alpha_s \nabla p - \nabla p_s + \nabla \cdot (\alpha_s \tau_s) + \alpha_s \rho_s g + \beta(U_g - U_s) \quad (4)$$

β is the interphase momentum transfer coefficient, which varies depending on the specific model. The equation to find β is given in Table 2.

The gas phase is assumed to behave as a Newtonian fluid, and its stress tensor is defined using the Newtonian stress–strain relation as

$$\tau_g = \mu_g \left[\nabla U_g + (\nabla U_g)^T\right] - \frac{2}{3}\mu_g (\nabla \cdot U_g) I \quad (5)$$

$$\tau_s = \mu_s [\nabla U_s + (\nabla U_s)^T] + \left(\lambda_s - \frac{2}{3}\mu_s\right)(\nabla \cdot U_s) I \quad (6)$$

To order to solve the phase momentum equations, the interphase momentum transfer coefficient (β) should be calculated with drag force functions. In this work, the drag force function of the Gidaspow model (Gidaspow, 1994) combines the Ergun equations (Ergun, 1952) with the Wen and Yu model (Wen, 1966). In the work of Y. Liu (Yefei Liu, 2014) drag force function of the Syamlal model (Syamlal 1993) is used. The correlations of the Syamlal and Gidaspow models are given in Table 2, respectively, also showing the comparison between these two models. According to Yefei Liu (2014), at high solid volume fractions, the values calculated with the Gidaspow model are larger than those calculated with the Syamlal model. Therefore, the Gidaspow model predicts stronger bed expansion, which will also be observed when comparing our result at Uair = 0.46 m/s velocity. The preliminary study done by Yefei Liu (2014) revealed that the fluidized bed with uniform gas feed is better simulated using the

Syamlal model. We would simulate different drag models and compare them with the experiment conducted by Fariborz Taghipour (2005) to get a better understanding.

Table 1: Coefficients of Governing equations.

ρ_g	gas phase density
ρ_s	solid phase density
U_g	gas phase velocity
U_s	solid phase velocity
α_g	volumetric fractions of gas
α_s	Volumetric fractions of solid phases
p	the bed pressure

p_s	solid phase pressure
τ_g	stress tensors of gas
τ_s	stress tensors of solid phases
g	gravitational acceleration
μ_g	shear viscosity of the gas phase
μ_s	solid shear viscosity
λ	solid bulk viscosity

Table 2: The interphase momentum transfer coefficients

Syamlal model (Syamlal M, 1993)

$$\beta = \frac{3}{4} C_D \frac{\alpha_g \alpha_s \rho_g}{V_r^2 d_p} |U_g - U_s|$$

C_D	$\left(0.63 + 4.8\sqrt{\frac{V_r}{Re}}\right)^2$
Vr	$0.5\left[a - 0.06Re + \sqrt{(0.06Re)^2 + 0.12Re(2b-a) + a^2}\right]$
a	$\alpha_g^{4.14}$
b ($\alpha_g <= 0.85$)	$0.8\alpha_g^{1.28}$
b ($\alpha_g > 0.85$)	$\alpha_g^{2.65}$
Re	$\mathrm{Re} = \frac{\rho_g d_p \lvert U_g - U_s \rvert}{\mu_g}$

Gidaspow model (Gidaspow, 1994)

$$\beta = \frac{3}{4} \cdot \frac{C_D \alpha_g \alpha_s \rho_g |U_g - U_s|}{d_p} \alpha_g^{-2.65} \qquad \alpha_s < 0.2$$

$$\beta = 150 \cdot \frac{\mu_g \alpha_s^2}{\alpha_g d_p^2} + 1.75 \cdot \frac{\rho_g \alpha_s}{d_p} |U_g - U_s| \qquad \alpha_s \geq 0.2$$

C_D	$\frac{24}{\alpha_g Re}\left[1 + 0.15(\alpha_g Re)^{0.687}\right] \qquad \alpha_{g\mathrm{Re}} < 1000$
C_D	$0.44 \qquad \alpha_{g\mathrm{Re}} \geq 1000$

The solid shear stress τ_s and solid pressure p_s in Eq. (4) are modelled by the kinetic theory of granular flow Gidaspow (1994). The fluctuation energy of the solid phase, also known as the granular temperature, is obtained by solving its transport equation:

$$\frac{3}{2}\left[\frac{\partial}{\partial t}(\alpha_s\rho_s\Theta)+\nabla\cdot(\alpha_s\rho_s U_s\Theta)\right]=(-p_s I+\tau_s):\nabla U_s+\nabla\cdot(\kappa_s\nabla\Theta)-\gamma_s+J_{\text{vis}}+J_{\text{slip}} \quad (7)$$

$$\lambda_s(Solid\ collision\ viscosity)=\frac{4}{3}\alpha_s\rho_s d_p g_0(1+e)\left(\frac{\Theta}{\pi}\right)^{1/2} \quad (8)$$

The solid bulk viscosities and the solid shear viscosities μ_s are calculated according to Gidaspow (1994).

$$\mu_s=\frac{4}{5}\alpha_s^2\rho_s d_p g_0(1+e)\left(\frac{\Theta}{\pi}\right)^{1/2}+\frac{10\rho_s d_p\sqrt{\Theta\pi}}{96 g_0(1+e)}\left[1+\frac{4}{5}\alpha_s g_0(1+e)\right]^2 \quad (9)$$

The solid phase pressure p_s is calculated following the work of Lun et al. (1984):

$$p_{s,\text{KTGF}}=\alpha_s\rho_s\Theta[1+2(1+e)g_0\alpha_s] \quad (10)$$

The expression of g_0, which indicates the radial distribution function, proposed by Sinclair and Jackson (1989) is used:

$$g_0=\left[1-\left(\frac{\alpha_s}{\alpha_{s,max}}\right)^{1/3}\right]^{-1} \quad (11)$$

where $\alpha_{s,\ max}$ is the maximum particle packing limit in our case is 0.65. In OpenFOAM, the value of g_0 must be specified by the user; by putting the value given in the table, the value of g_0 is approximately 38. This value must be specified by the user in OpenFOAM.

The behaviour of granular flow is primarily governed by frictional stresses when particles are closely packed. Similar to solid kinetic stresses, frictional stresses in solids comprise both frictional shear stress and frictional normal stress. When the solid volume fraction exceeds a critical value $\alpha_{s,\ min}$ (AlphaMinFriction), the frictional stresses are typically incorporated into the solid kinetic stresses calculated using the Kinetic Theory of Granular Flow (KTGF) (Johnson, P.C., 1990).

$$p_s=p_{s,\text{KTGF}}+p_{s,f} \quad (12)$$

$$\mu_s=\mu_{s,\text{KTGF}}+\mu_{s,f} \quad (13)$$

The solid frictional pressure, $p_{s,f}$, proposed by Schaeffer (1987), and the

$$p_{s,f}=Fr\frac{(\alpha_s-\alpha_{s,min})^2}{(\alpha_{s,max}-\alpha_s)^5} \quad (14)$$

Solid frictional shear viscosity $\mu_{s,f}$ by (Johnson P.C, 1990) are employed as

$$\mu_{s,f} = \frac{p_{s,f} \sin \phi_{fr}}{2\sqrt{I_{2D}}} \quad (15)$$

where Fr represents the Frictional stress coefficient and ϕ_{fr} = 28.5 degrees.

Table 3: Coefficient of the Constitutive equation.

θ	Granular temperature
κ_s	Conductivity of granular temperature
γ_s	Dissipation rate due to particle collisions
J_{vis}	Dissipation rate resulting from viscous damping
J_{slip}	Production rate due to the slip between the gas and the particle
d_p	Particle diameter
e	Particle–particle restitution coefficient
ϕ_{fr}	Internal frictional angle

4. Simulation Procedure

4.1 Geometry and mesh

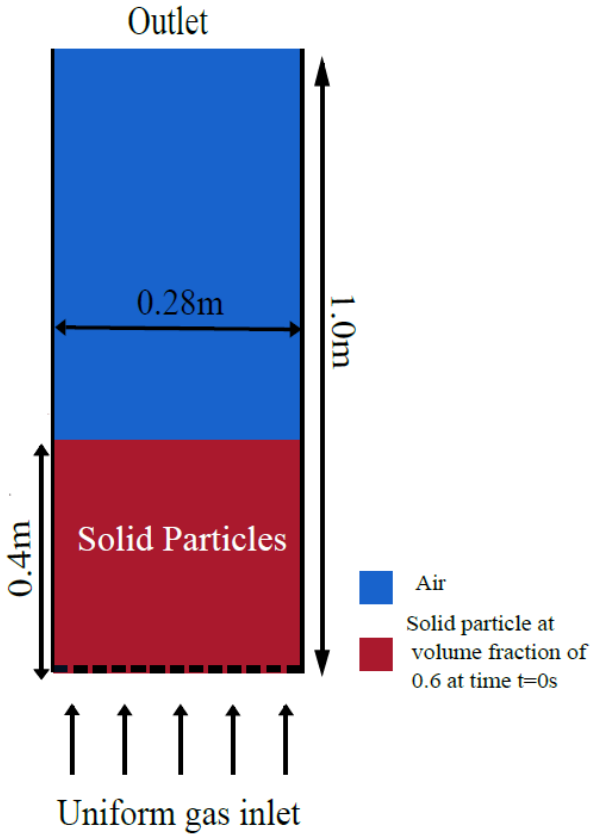

Figure 2: Schematics of a Fluidized bed at t = 0 sec, showing dimensions and initial particle arrangement.

A 3D domain is created using "blockMesh" as OpenFOAM can only support 3D geometry but the changes in properties along the z-axis will not be considered for a fluidized bed hence, the geometry can be considered as a 2D domain with a uniform gas inlet from the bottom, and is discretized into 11200 rectangular cells. The geometry and setup are similar to those used by Fariborz Taghipour (2005) and Yefei Liu (2014). Figure 2, which accompanies this text, shows the schematics of the fluidized bed created with open-source software Inkscape. It provides a schematic representation of the fluidized bed and its dimensions. In this work, the time step is set to 1.0 x 10^{-3} s to minimize computational costs. The other parameters of air, particle and the fluidized bed are shown in Table 5.

At time t = 0, the solid particle is located below the bed at a covering height of 0.4 meters, with a solid volume fraction of 0.6. In the solid state, different types of solid arrangements exhibit various packing efficiencies. These arrangements include Hexagonal Close Packing (HCP), Face-Centred Cubic (FCC), and Body-Centred Cubic (BCC). HCP and FCC have a packing fraction of 74%, while BCC has a packing fraction of 68%.

The higher packing fractions observed in HCP and FCC can be attributed to several assumptions that do not account for forces of attraction or repulsion. Additionally, packing efficiency is reduced due to random packing. Consequently, a general case of 60% packing efficiency is considered. At t = 0 seconds, from a height of 0 meters to 0.4 meters, there is 60% solid particle volume and 40% air filling the voids.

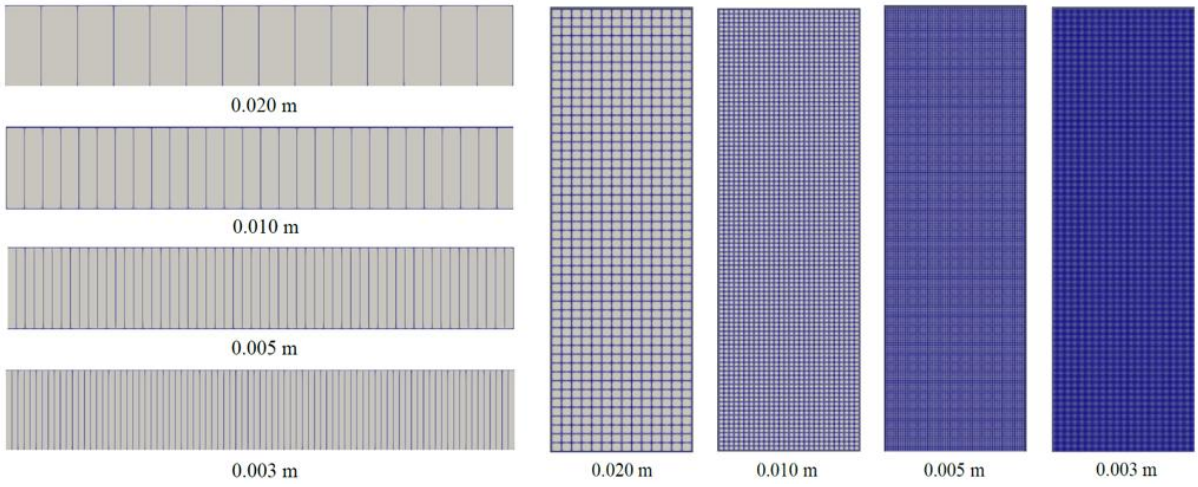

Figure 3: Schematics of a Fluidized bed with different grid sizes

In the simulation performed by Fariborz Taghipour (2005), Yefei Liu (2014), Fatti & Fois (2020-21), all of them have used a square grid size of 0.005 m. To ensure our results are comparable to theirs and experimental data, we will also use a 0.005 m grid in our simulation.

To assess the impact of grid size on the results, specifically on the solid volume fraction, additional simulations will be conducted using various grid sizes. We will then compare these results to one another to analyse the changes that occur when the grid size is altered.

4.2 Initial and final boundary Conditions

4.2.1 Selection of Boundary Conditions in OpenFOAM for Solid Volume Fraction of air and particle.

Applying appropriate boundary conditions is critical for accurate fluidized bed simulations in OpenFOAM for achieving realistic and stable results. Two commonly used boundary conditions while simulating a fluidized bed are the fixedValue and zeroGradient boundary conditions. In fluid dynamics, a gradient refers to the rate of change of a variable (such as velocity, pressure, or temperature) with respect to distance in a certain direction. The zeroGradient boundary condition assumes that there is no change in the value in the direction normal (perpendicular) to the boundary. The fixedValue boundary condition, on the other hand, is used when we want to set a value for a variable at the boundary. This is known as a Dirichlet boundary condition. For example, you might use fixedValue to set a constant velocity at the inlet of a fluidized bed or to set the temperature at a wall.

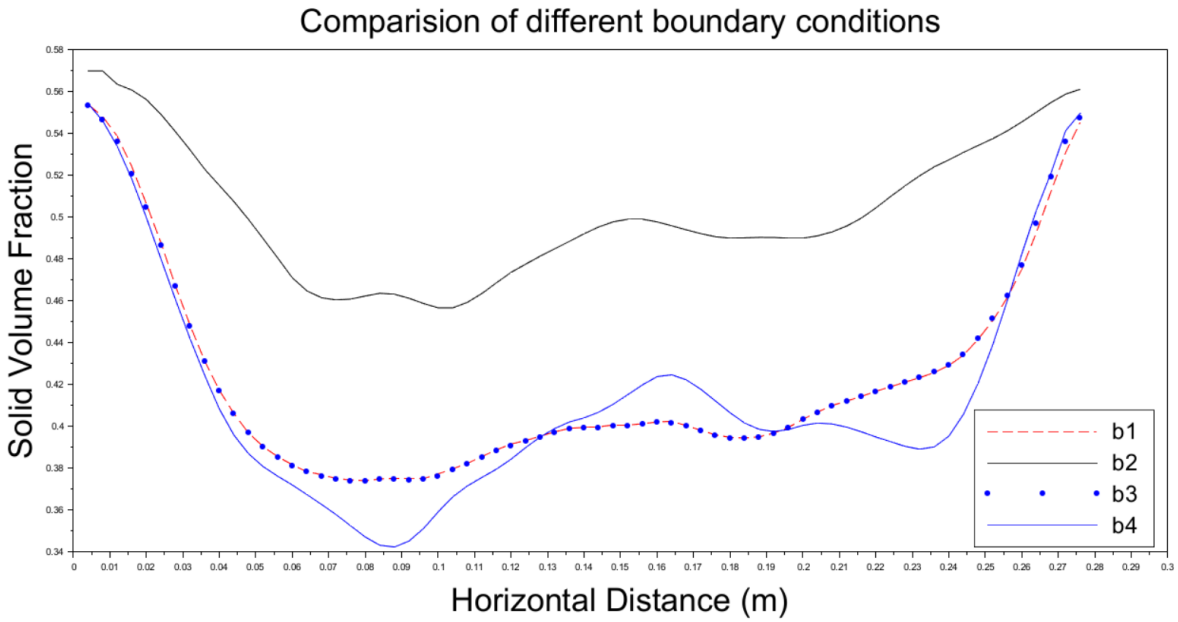

Figure 4: Comparison of different inlet boundary conditions of solid volume fraction.

Table 4: Different inlet boundary conditions of air and particles.

	Alpha. Air	Alpha. Particle
b1	fixedValue	fixedValue
b2	fixedValue	zeroGradient
b3	zeroGradient	fixedValue
b4	zeroGradient	zeroGradient

The remaining boundary conditions, including the outlet conditions for the solid volume fraction and other related parameters, are consistent with those specified by Fatti&Fois (2020-21).

According to Fariborz Taghipour (2005) and (Yefei Liu (2014) simulation result when (Uair = 0.38 m/s), the solid volume fraction of particle must lie between 0.58 to 0.45 and only one condition is making this satisfied, which is b2, where the inlet boundary condition of air is fixed value and inlet boundary condition of particle is zero gradient hence we can say that external air must enter the fluidized bed. The condition considered by Fatti&Fois (2020-21), where they performed a simulation using the b4 condition also compared with the results of Fariborz Taghipour (2005).

For our study to get the best data, we will take the b2 case, and all the changes in the drag model and velocities will be done in the b2 case.

4.2.2 Numerical implementation

The PIMPLE algorithm is used here in these simulations; it is a mixture of the PISO and methods. The PISO algorithm was used by Yefei Liu, (2014). It is particularly useful for solving pressure-velocity coupling in transient simulations, such as those involving fluidized beds. These systems often exhibit strong phase interactions and require large time steps, making PIMPLE a preferred choice over pure PISO due to its incorporation of under-relaxation, a feature borrowed from SIMPLE, which enhances numerical stability.

PIMPLE is especially well-suited for simulating fluidized beds due to the fast transients involved, such as bubble formation and particle clustering. The use of large time steps (10^{-3} in our simulation) can often lead to divergence, but PIMPLE's stabilizing mechanisms help mitigate this risk. For these reasons, OpenFOAM's *twoPhaseEulerFoam* solver, commonly used for gas-solid flows, typically employs the PIMPLE algorithm to handle the complex dynamics of fluidized bed systems effectively.

4.2.3 Different turbulence, thermophysical properties, and models of Gas and Particles

For performing a simulation, we need to input many values for different turbulence and thermophysical properties of air and particles, which also have a critical influence on the final result in solid volume fraction. This value will remain constant even when we change the velocity, grid size, and time step.

The inlet is impermeable to solids, while airflow is allowed. The solid volume fraction (specified in the *alpha.air* file) is set to 1 at the inlet, and the air velocity is assigned values of 0.38 m/s and 0.46 m/s for two different cases. The particle velocity is set to zero, indicating that any subsequent change in particle velocity will result from drag forces caused by the air's momentum. A no-slip boundary condition is applied to the air at the wall, ensuring that the relative velocity between the air and the wall is zero. For the solid phase, a partial slip boundary condition is applied, as proposed by Johnson and Jackson (1987). According to them, the velocity of the particle at the surface is determined by,

$$\nabla\tau_{s,w} = -\frac{\pi}{6}\frac{\alpha_s}{\alpha_{s,\max}}\psi\rho_s g_0\sqrt{3\Theta}U_{s,w} \qquad (18)$$

Where ψ The specularity coefficient is when its value is zero, which means a perfectly smooth surface exists, and unity represents a no-slip boundary condition.

Table 5: Value of different thermophysical parameters and Coefficients.

Parameters	Value
Bed depth (z axis), m	0.025
Initial bed height, m	0.4
Initial solid Packing fraction	0.6
Gas density, kg/m^3	1.2
Molecular Weight of air kg /mol	28.9
Temperature of gas, K	300
Temperature of particle, K	300
Particle diameter, m	2.8 * 10^{-4}
Particle density, kg/m^3	2500
Min solid volume fraction	0.5

Parameters	Value
Specific Heat Capacity of particle J/kgK	800
Molecular weight of the particle kg/mol	60.08
Heat of formation J/kg	0
Prandtl no. for air	0.7
Viscosity of air	1.81 * 10^{-5}
Specific Heat Capacity of air Kg/m3	1007
Prandtl number for particle	1

Johnson-Jackson coefficient	Value
Frictional stress coefficient (Fr)	0.05
Frictional exponent	2
Specularity exponent	5
Specularity coefficient	0.5
Threshold for frictional stress activation	0.05

Phase pressure coefficient	Value
Pre-exponent factor	500
Exponent for pressure term	1000
Max. Packing fraction	0.65
Radial distribution function	38

Kinetic theory coefficient	Value
Restitution coefficient	0.8
AlphaMinFriction	0.5
residualAlpha	10^{-4}

Table 6: Selected models for various parameters

Sr no.	Parameters	Models used in this work
1.	Viscosity	Gidaspow
2.	Conductivity	Gidaspow
3.	Granular pressure	Lun
4.	Frictional stress	JohnsonJackson
5.	Radial	SinclairJackson

4.3 Solver

There are several methods to simulate two-phase flow using CFD, such as the Eulerian–Eulerian approach, the Eulerian–Lagrangian approach, and hybrid methods. The Eulerian–Eulerian approach, also known as the two-fluid method, treats both phases as interpenetrating continua, where both phases coexist within the computational domain. Although the solid phase consists of discrete particles, it is modeled as a continuous medium, and the solver computes the Navier–Stokes equations for both phases while accounting for differences in physical properties such as density, viscosity, and heat capacity. To close the governing equations, additional closure models are required to describe interphase momentum, heat, and mass transfer. The choice of these closure models can influence the accuracy of the results, although the overall trends generally remain consistent.

In contrast, the Eulerian–Lagrangian approach treats the gas phase as a continuum and the solid phase as a collection of discrete particles. In this method, the fluid flow is solved on a fixed computational grid using continuum equations, while the motion of individual particles is tracked by solving Newton's second law of motion for each particle. Although Eulerian–Lagrangian models provide a more detailed representation of particle behavior, they are computationally expensive, especially when simulating systems with millions of particles (Fariborz Taghipour, 2005). Consequently, the Eulerian–Eulerian continuum approach is commonly employed for fluidized bed simulations (Pain et al., 2001). In this work, the solver used for simulating the fluidized bed is twoPhaseEulerFoam in OpenFOAM, which, as the name suggests, treats both phases as interpenetrating continua.

5. Results and discussions

The fluidized bed was simulated for 60 s in real time, and a time average of 55s is taken to plot the graph, similar to the way plotted by Yefei Liu (2014). Post-processing is performed in Paraview, where the results contour is visualized, and the graph is plotted using the "Plot Over Line" tool. This tool provides all the data at every single point on the line. The solid volume fraction fields are then identified. The line that was drawn was a horizontal line at a distance of 0.2 m above the inlet.

As seen in Figure 5, the result obtained in this study for an air inlet velocity of 0.38 m/s shows closer agreement with experimental results compared to other simulations. The parameters were kept consistent with those mentioned Yefei Liu (2014). However, the drag model was changed to 'GidaspowErgunWenYu' in OpenFOAM's phase property files. To manage computational time, a time step of 10^{-3} was used, which took approximately 3.5 hours for a single simulation on a computer with an AMD Ryzen 5 processor. A similar time step was also used by Fariborz Taghipour (2005).

Observing the solid volume fraction data from x = 0.1 to x = 0.2, as presented in Table 5 and representing the middle of the horizontal axis, reveals significant variations. In contrast, the other regions of the plot outside x=0.1 m to 0.2 m exhibit a more uniform trend. The average solid volume fraction for the entire bed may not provide the most accurate assessment, as it includes portions where the variation is minimal. Along the horizontal axis, the solid volume

fraction starts at 0.58, decreases to 0.40, and then increases again to 0.58 toward the end of the bed. This pattern is consistent across all simulation plots. Therefore, the data from the middle section of the bed are considered more relevant when evaluating the accuracy of the results. For this velocity, the simulation was performed only using the Gidaspow model, as it provided a trend closely matching the experimental results, as shown in Figure 5.

Table 7: Average of solid volume fraction for different results at Uair =0.38 m/s.

	Total average of solid volume fraction	**Average of solid Volume fraction from x=0.1 m to x=0.2 m**	**% Difference from the experimental data. (Considering the middle data of the horizontal axis)**
(Yefei Liu, 2014)	0.486567	0.455144	8.12424
(Fariborz Taghipour, 2005)	0.489438	0.465476	5.72425
This work	0.502517	0.503347	2.230271 (Least difference – Most accurate)
Experimental	0.501093	0.492124	

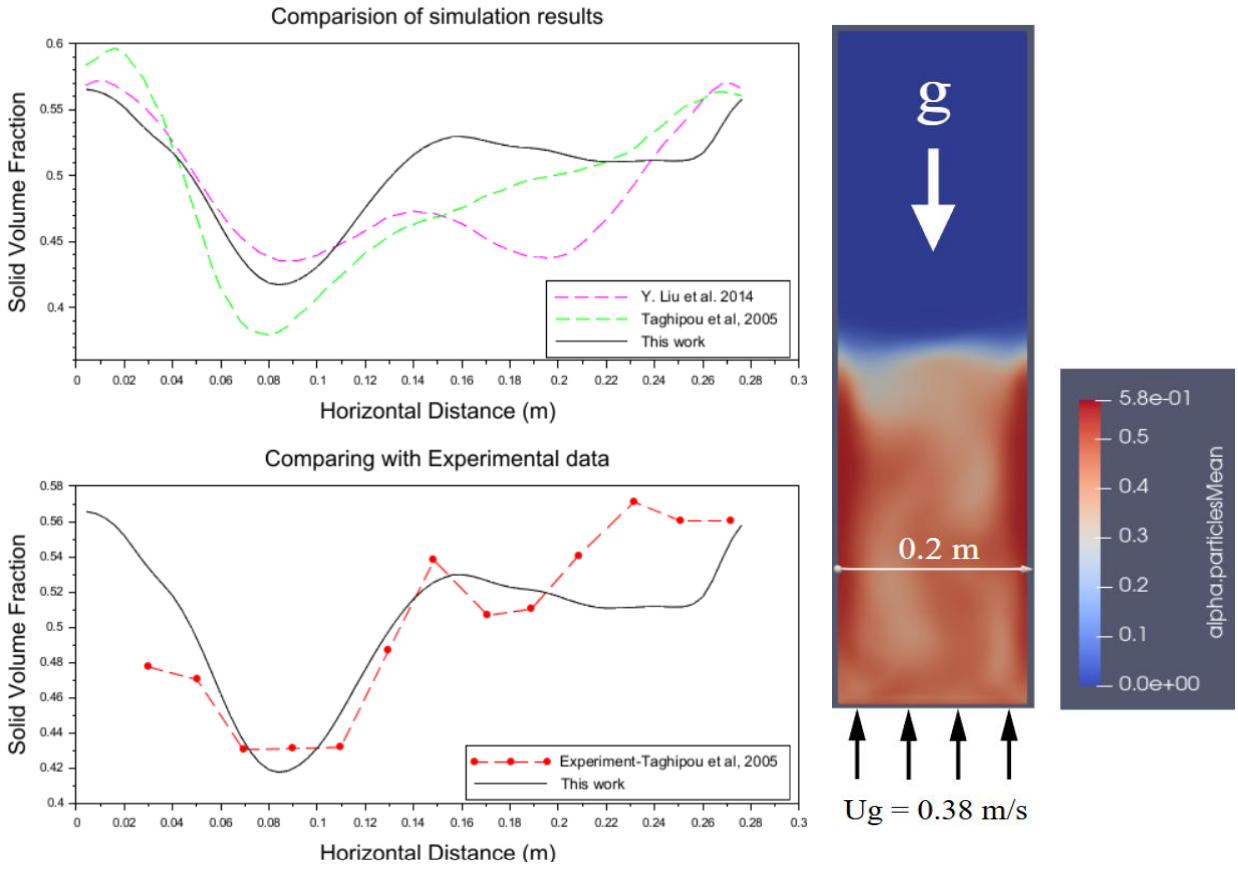

Figure 5: Comparison of average solid volume fraction between this study, experimental data, and previous simulations at U_air = 0.38 m/s.

The average data in the middle of the horizontal axis shows that the results from this work are the closest to the experimental data when compared to the other data. This can also be observed in the graphical plot shown in Figure 5.

When the inlet velocity is increased to 0.46 m/s, the solid volume fraction profile changes noticeably. To simulate this scenario, two drag models, GidaspowErgunWenYu and SyamlalO'Brien, were employed, and their respective results are presented. As shown in Figure 6, the bed expansion predicted in this study remains relatively low for both drag models under these conditions. The reason for selecting two different drag models at this velocity is that, unlike the case with 0.38 m/s, the graphs do not align as closely, making it beneficial to compare the predictions using two distinct models, one of which was originally proposed by Yefei Liu, (2014) (SyamlalOBrien) and the other taken by Fatti and Fois (2020-21) (GidaspowErgunWenYu) for caring there simulation.

The simulation results of Fariborz Taghipour (2005) differ significantly from the experimental results. This difference may be attributed to the selection of the coefficient of restitution, which he set at 0.9 and 0.99. This is higher than the value of 0.8 used Yefei Liu, (2014), which results in better simulation results than Fariborz Taghipour 2005 simulation results. According to Taghipour, increasing the value from 0.9 to 0.99 results in an increase in bed height from 1.35 to 1.45, thereby reducing the solid volume fraction. The value of 0.99 represents an ideal condition, typically observed when the bed is less dense, as reflected in the corresponding graphs.

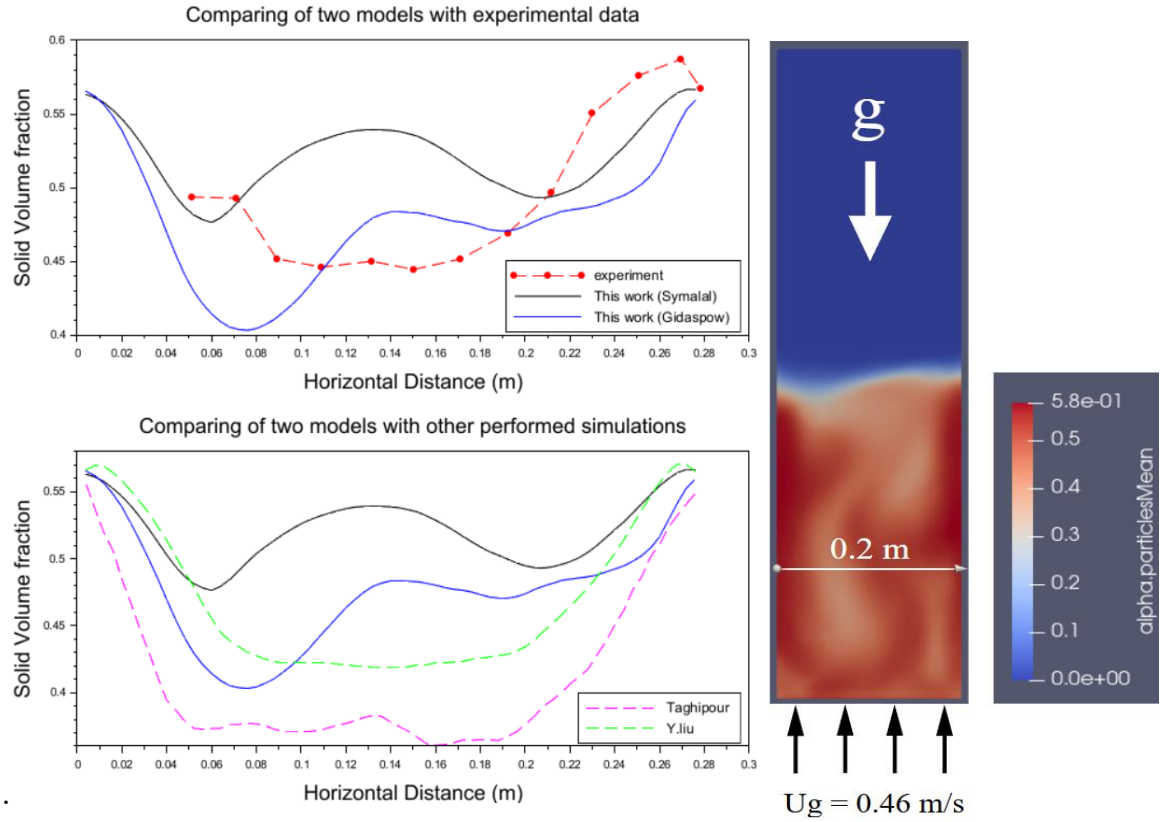

Figure 6: Comparing the average solid volume fraction with experimental and other simulation data (Uair = 0.46 m/s)

According to the table, the (Gidaspow, 1994) model exhibits a lower solid volume fraction than the experimental data, indicating greater drag and, consequently, more bed expansion. This supports the assertion that the Gidaspow model predicts more bed expansion, possibly due to the neglect of van der Waals forces.

Table 8: Average of solid volume fraction for different results at Uair =0.46 m/s

	Total average of solid volume fraction	**Average solid volume fraction from x=0.1m to x=0.2m**	**% Difference from the experimental data (Considering the middle data of the horizontal axis)**
(Yefei Liu, 2014)	0.486567	0.422978	8.67
(Fariborz Taghipour, 2005)	0.489438	0.370703	24.00
This work (Gidaspow)	0.47634435	0.46967608	2.13 (Least difference – Most accurate)
This work (Symalal)	0.521167	0.52477	12.41
Experimental	0.498291	0.45965608	

Similar to the case Uair = 0.38m/s, only data from the mid-section of the horizontal axis are considered. The results obtained using the Gidaspow drag model show better correlation with experimental data compared to the Syamlal-O'Brien model and other simulations. Although the experimental and simulated curves do not perfectly overlap, the average solid volume fraction along the mid-section indicates that our predictions are more accurate on an overall basis. Perfect curve matching is not essential; rather, the goal is to achieve symmetry and ensure the simulated results remain close to experimental data within an acceptable range.

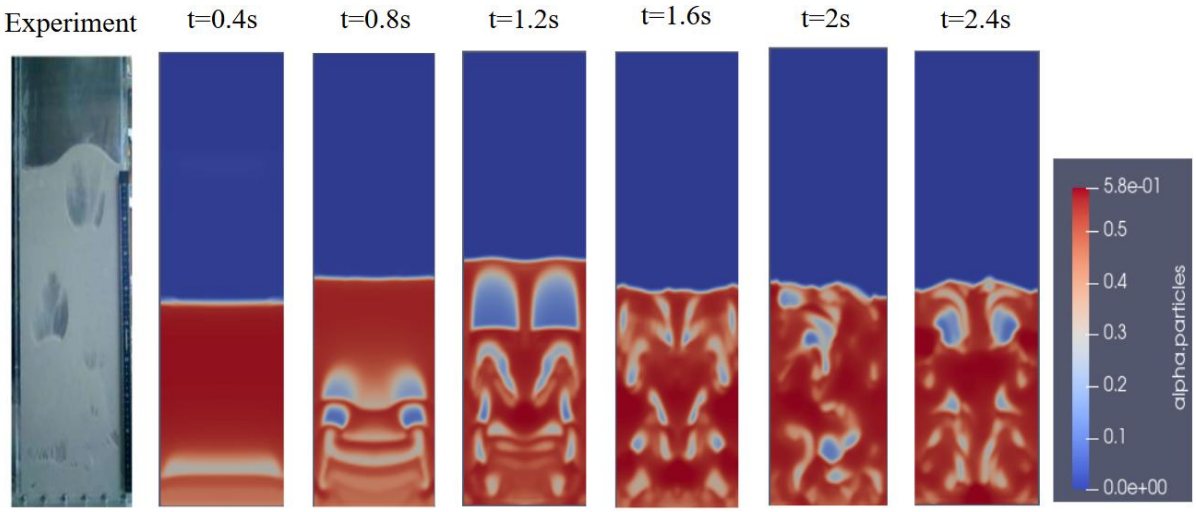

Figure 7: Snapshot of experiment of Fariborz Taghipour, 2005 and simulated solid volume fraction (Ug=0.46 m/s)

While simulating the results of velocities, we used a grid size of 0.005 m, which is consistent with other simulations we have performed. However, we understand that in computational fluid dynamics (CFD), the mesh size can significantly impact the results. To investigate this further, we will test different grid sizes and compare them to see if and how much they differ from the original results.

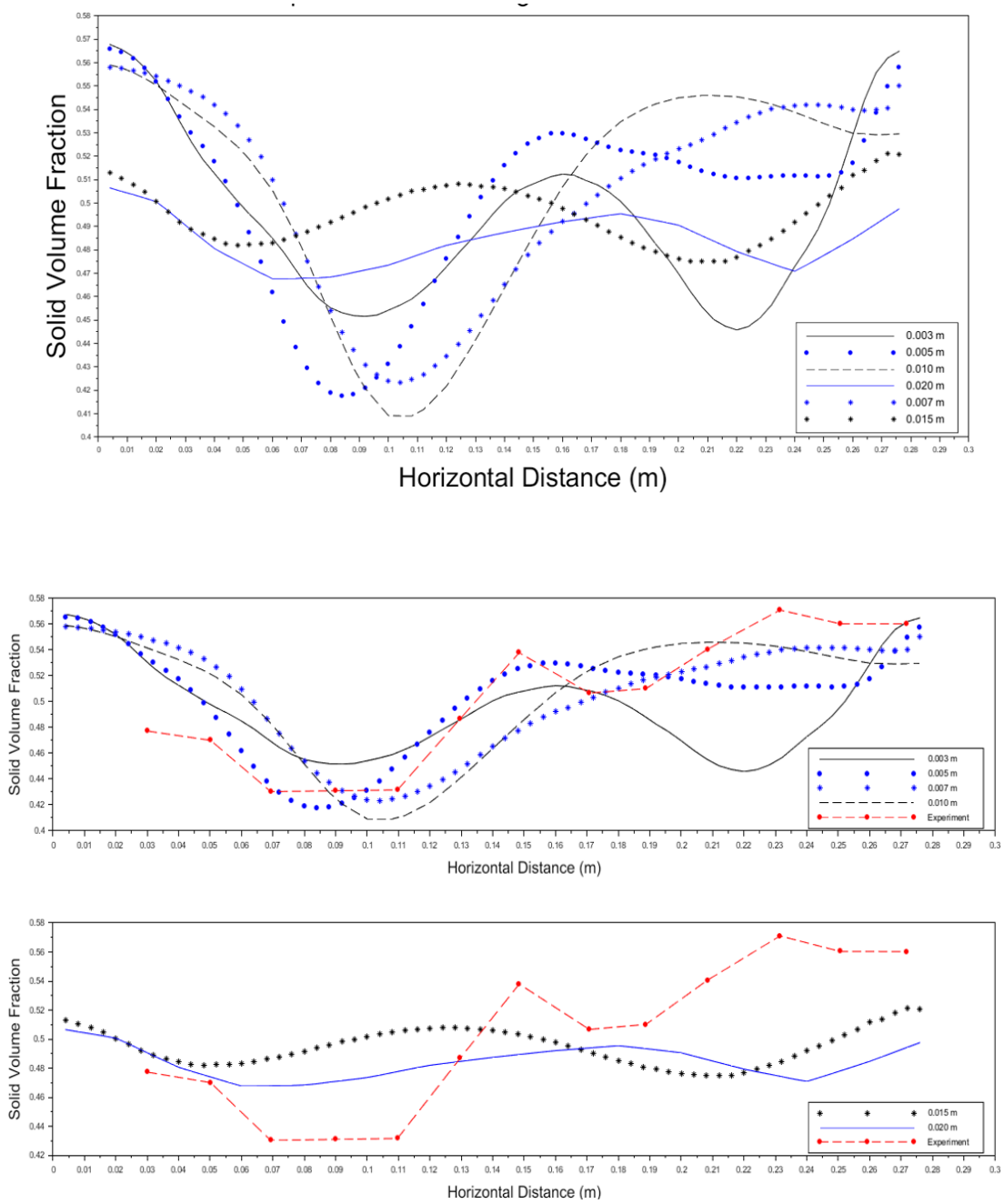

Figure 8: Comparing solid volume fraction at Uair = 0.38 m/s at different grid sizes and with experimental plot.

In Figure 8, we observe that the solid volume fraction line for larger grid sizes of 0.02 m and 0.015 m has a very narrow range at the wall edge, where it maintains a value of 0.55, even when particles slide near the wall, according to the Johnson and Jackson (1987) boundary condition.

For the smaller mesh size of 0.003 m, the plot appears more symmetrical, which would represent the ideal situation if the velocity inlet were uniform. Additionally, all results for grid sizes larger than 0.01 m exhibit the same range for the solid volume fraction. To establish an appropriate range for the solid volume fraction, we need to select a suitable grid size to minimize computational costs. However, to enhance our understanding of the conditions, a finer mesh is advisable. Thus, we can conclude that the results are more reliable when the bed height falls within a specific range. To verify the accuracy of the results, we need to check the minimum bed height at various distances along the x-axis.

From the above observations, it is evident that a grid size of 0.003 m provides better bed expansion compared to the original grid size of 0.005 m. The results for grid sizes of 0.015 m and 0.020 m are entirely incorrect, as the solid volume begins at 0.5 m at the walls, whereas it should start at 0.58 m, which is also indicated in the experimental data at 0.28 m. Similar trends can be noted for Uair = 0.46 m/s, shown in Figure 9.

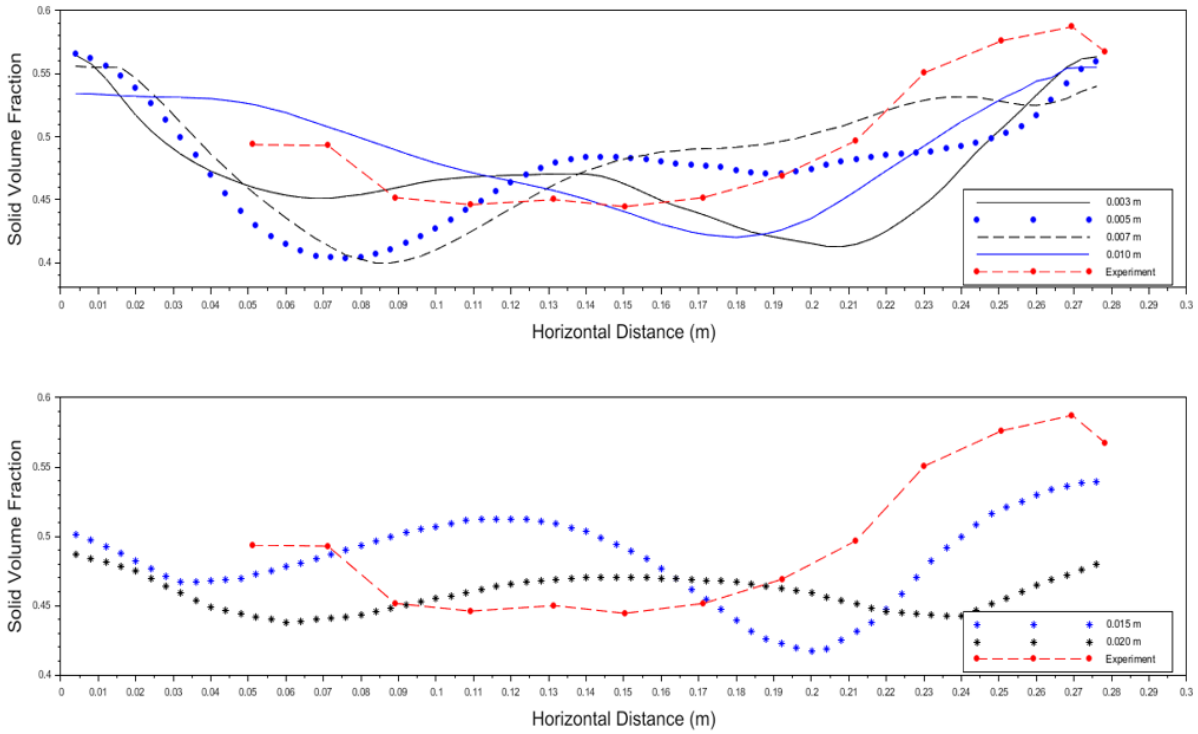

Figure 9: Comparing solid volume fraction at U air = 0.46 m/s of different grid sizes with experimental plot.

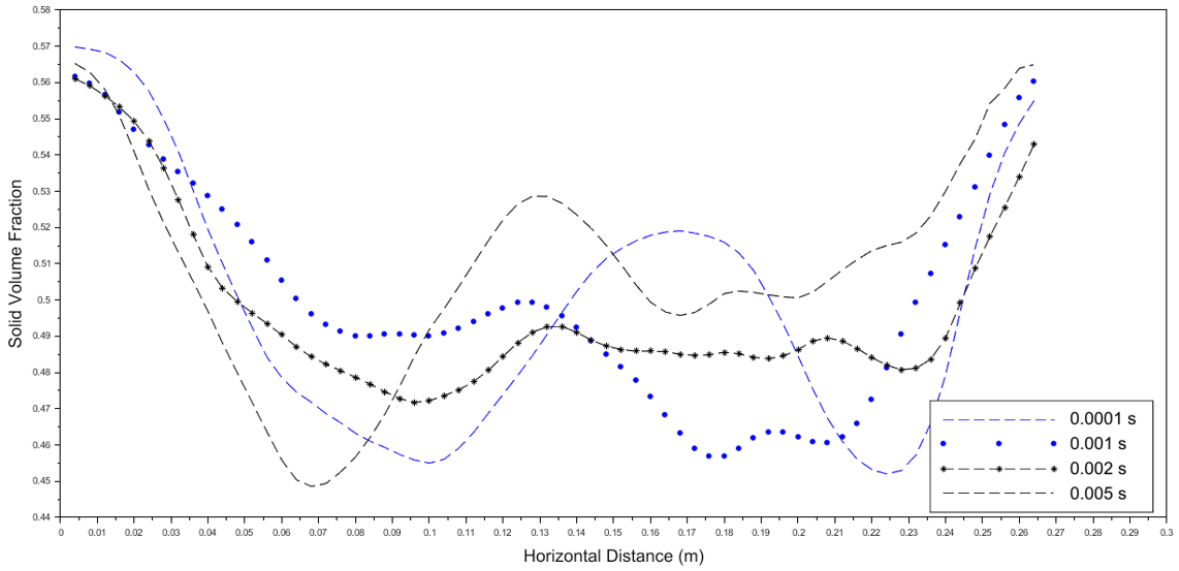

Figure 10: Comparison of solid volume fraction of Solid Particle (Uair = 0.38 m/s) at different time steps.

Similar to the effect of grid size, reducing the time-step size produces a more symmetrical plot, which represents the ideal case and suggests improved results. While this may not always hold in practice, theoretically, decreasing the time step should yield values that are closer to the ideal plot (Which must actually happen in a real case).

Table 9: Time required at different time steps for a 12-second simulation.

Time step	**Time taken for simulation (in seconds)**	**Time taken for simulation (in hours)**
0.0001	16381	4 hrs 33min
0.0005	4264	1 hr 11min
0.001(This work)	2772	46 min
0.002	1440	24 min

The above plot in Figure 10 was simulated for 12 seconds, with our time step size of 0.001 s and a square grid size of 0.005m. It takes 30 minutes for a 12-second simulation. For a 60-second simulation, it would take 230 minutes, which is close to 3 hrs 50 minutes. Time step was taken as 10^{-5} by Fatti and Fois, which can take weeks, as a tenfold decrease in time step increases the computation time by approximately a factor of six. Therefore, selecting an appropriate time step similar to the careful selection of the grid size is essential for better computational efficiency. It is possible that with an even smaller time step, such as the simulation results at 60 seconds, could closely match the experimental data. However, this aspect was not within the scope of the present study. Additionally, minor errors in experimental measurements cannot be ruled out. Therefore, it is always advisable to consider both accuracy and computational time when determining the appropriate time step.

6. Conclusion

This study successfully demonstrated the application of the Eulerian–Eulerian two-fluid model in OpenFOAM for simulating gas–solid hydrodynamics in a bubbling fluidized bed. By systematically evaluating drag models, boundary conditions, grid sizes, and time step sensitivities, the work identified the critical factors influencing simulation accuracy and stability.

Comparisons with experimental and simulation data from Taghipour (2005) and Y. Liu (2014) revealed that the Gidaspow drag model generally provides better agreement for mid-bed solid volume fractions at lower inlet velocities, while the Syamlal–O'Brien model tends to overpredict bed expansion at Uair =0.46 m/s. while for velocity of Uair =0.38 Gidaspow model gives an accurate trend similar to the experimental data. The boundary condition combination of fixedValue for the gas phase and zeroGradient for the solid phase at the inlet produced results consistent with physical expectations.

Mesh and time-step analyses confirmed that finer grids and smaller time steps yield improved agreement with experiments, though at the expense of higher computational cost. A balanced choice of 0.005 m grid size and 10^{-3} s time step was found to provide acceptable accuracy within practical runtimes.

Overall, the findings highlight the importance of selecting appropriate drag models, boundary conditions, and numerical parameters for reliable fluidized bed simulations.

7. References

Ergun. (1952). Fluid flow through the pack column. Chemical engineering process.

Fariborz Taghipour, N. E. (2005). Experimental and computational studies of gas-solid fluidized bed hydrodynamics. Elsevier.

Fatti&Fois. (2020-21). CFD modeling of gas-solid fluidized beds in OpenFOAM:.

Gidaspow, D. (1994). Multiphase flow and fluidization. Academic Press.

Johnson P.C, J. R. (1990). Frictional-collisional equations of motion for particulate flows and their application to chutes. Journal of Fluid Mechanics.

Syamlal M, W. R. (1993). MFIX Documentation Theory Guide. osti.gov.

Wen CY, Y. Y. (1966). Mechanics of fluidization.

Yefei Liu, O. H. (2014). CFD modeling of bubbling fluidized beds using OpenFOAM ®: Model validation and comparision of TVD differencing schemes.

Johnson PC, Jackson R. Frictional–collisional constitutive relations for granular materials, with application to plane shearing. Journal of Fluid Mechanics 1987